

More power on large scales

Jeremy Mould^{1,2}

¹ Swinburne University, PO Box 218, Hawthorn 3121, Australia

² ARC Centre of Excellence for Dark Matter Particle Physics
 e-mail: jmould@swin.edu.au

Received November 30, 2025

ABSTRACT

The high value of the cosmic microwave dipole may be telling us that dark matter is macroscopic rather than a fundamental particle. The possible presence of a significant dark matter component in the form of primordial black holes (PBHs) suggests that dark halo formation simulations should be commenced well before redshift $z = 100$. Unlike standard cold dark matter candidates, which are initially relativistic or possess thermal velocities, PBHs behave as dense, non-relativistic matter from their inception in the radiation-dominated era. This allows them to seed gravitational potential wells and begin clustering much earlier, significantly altering the initial power spectrum on small scales. We find that starting N-body simulations at redshifts even before matter-radiation equality ($z \sim 3400$) yield galaxy bulk flow velocities that are systematically larger than those predicted by standard Λ CDM models. The early, high-mass concentrations established by PBHs lead to a more rapid and efficient gravitational acceleration of surrounding baryonic and dark matter, generating larger peculiar velocities that remain coherent over scales of hundreds of Mpc. Furthermore, a sub-population of PBHs in the 10^{-20} to $10^{-17} M_\odot$ mass range would lose a non-negligible fraction of their mass via Hawking radiation over cosmological timescales. This evaporation process converts matter into radiation, so a time-varying matter density parameter, Ω_m' , is introduced, which behaves like a boosted radiation term, in the Friedmann equation. This dynamic term, which is most active between recombination and the late universe, acts to reduce the Hubble tension. A higher effective Ω_r in the early universe (pre-evaporation) reduces the sound horizon at the epoch of recombination. This smaller "standard ruler," as imprinted on the cosmic microwave background (CMB), would result in a higher value of the Hubble constant (H_0) inferred from the CMB at the 1% level, bringing it into slightly closer agreement with local, late-time measurements. PBH mass loss also influences fits to the equation of state parameter, w , at low redshift. The naive N-body modelling presented here suggests investigation with tried and tested cosmology codes should be carried out, by introducing mass losing PBHs and starting the evolution as early as practicable.

Key words. Primordial black holes(1292) – Cosmology(343) – Large-scale structure of the universe(902)

1. Introduction

Ever since peculiar velocities have been measured for galaxies, it has been noted that standard cosmological models lack sufficient power on large scales (Aaronson et al. 1988, Dekel 1993, Lauer & Postman 1994, Tully 1989, Hudson et al. 2004, Watkins et al. 2023, Whitford et al. 2023, Böhringer et al. 2025, Se-crest et al. 2025). Bouillot et al. (2014) find that the large bulk flow is due to an asymmetric distribution of matter, a rare event which would occur in the Λ CDM cosmology 1.4% of the time. Although the research is almost unanimous¹ on this issue, cosmological models that satisfy the constraint have not, with the possible exceptions of neutrinos and modified gravity², been forthcoming. Tsagas, Perivolaropoulos & Asvesta (2025) provide the most recent review. Even though the statistics will soon be overwhelming due to the WALLABY survey (Colless 2024), the DESI collaboration (2025) and 4HS (Taylor et al. 2023), there remain issues, such as Malmquist bias, that can afflict the data.

Here a toy model is offered that does develop higher velocities by employing mass losing dark matter and an early phase of high density (§2). If the dark matter (DM) particle is in fact

unstable, the decay products could be observed as an excess in the cosmic-ray fluxes of antimatter particles, γ -rays or neutrinos over the expected backgrounds. Many experiments have provided data of exquisite quality on the cosmic antimatter, γ -ray and neutrino fluxes, which allow us to set independent limits on the DM decay width into a given final state. Focussing on DM particles with masses in the GeV–TeV range, masses, m , from 10^{-2} to 10^7 GeV have σv cross-sections less than $10^{-22} \text{ cm}^3 \text{s}^{-1}$ (Pérez de los Heros 2020). With $v^2 = 2kT/m$ the decay rate, $n \sigma v$, for keV intergalactic medium temperatures and densities is less than 10^{-25} s^{-1} and for interstellar medium meV temperatures and GeV/cm^3 densities is less than a hundredth of that. DM particles in this range would therefore be stable at cosmic densities for a Hubble time. Still open to investigation, however, is dark matter decay beyond the standard model (e.g. Poulin, Desgourges & Serpico 2017).

Primordial black holes (PBHs), on the other hand, also decay into high energy photons and PeV to meV particles, depending on their mass, but experimental constraints have left open significant windows, notably between 10^{-16} and $10^{-8} M_\odot$. Those with $m < 10^{-19} M_\odot$ evaporate within a Hubble time (Mosbach & Picker 2022, Mould 2025). In §3 the toy model is normalised to observations. Simulated bulk flows are discussed in §4.

¹ An exception and a partial exception is work by Scrimgeour et al. (2016) and Courtois et al. (2025)

² Reviewed by Di Valentino, Perivolaropoulos and Said (2024).

2. A toy model

The best-motivated candidates for mass-losing DM are PBHs in the mass range of 10^{-20} - $10^{-17} M_{\odot}$, which would be losing mass via Hawking radiation on cosmological timescales (Figure 1).

A number of 256,000 particle n-body runs were made whose details are in Table 1 and whose final velocity distribution functions are in the Appendix. These are DM-only simulations. The run numbers are an internal reference code. The numerical resolution is a minimum particle distance of 10^{-20} . The PBHs expand with the Hubble flow. Black hole mergers are not treated, as they only become significant at supersolar PBH masses, where the geometrical cross-sections exceed 1 cm^2 . The initial conditions were a uniform random distribution of particles at rest in a sphere with a nucleus of mass m , the largest in the distribution. The simulations were scale free in radius, mass, and velocity.

The IMF was a top hat in log m with lowest and highest mass shown as m_1 and m_2 . Mould & Batten (2025) have shown that that IMF in the case of supermassive black holes yields the observed QSO luminosity function. The baryons are not considered in these calculations³.

Table 1: n-body simulations

Run	Initial z	m1	m2	dm/dt
102	10000	1	1	0.5%
103	10000	1	1	0%
104	30000	1	1	0.33%
105	30000	1	1	0%
106	3000	1	1	0.66%
107	3000	1	1	0%
108	10000	0.1	1	M&P
109	10000	0.1	1	0.5%
110	10000	0.1	1	M&P
111	10000	0.1	1	M&P
112	30000	0.1	1	M&P
113	10000	0.1	1	M&P
114	10000	0.1	1	0%
115	500	0.1	1	0%
116	100	10^{-6}	1	0%
118	2000	0.1	1	1%
117	15000	1	1	0.33%
119	500	0.1	1	1%
120	20000	0.1	1	M&P
121	5000	0.1	1	0.66%

M&P = Mosbach & Pecker mass loss
 dm/dt means mass lost per timestep

The toy model is implemented within a scale-free framework, which means that absolute masses, distances, and velocities are unspecified, but their ratios and the statistical properties of the density field are meaningful and can be scaled to any epoch where matter dominates. To quantify the resulting velocity field, we calculate the bulk flow from the particle velocity array. The median velocity is adopted as the primary statistic rather than the mean or *rms*, as it is more robust against spurious, high-velocity outliers generated by close two-body encounters, an unphysical artifact of N-body simulations at scales below the gravitational softening length.

³ Before recombination, the gas would be fully coupled to the radiation and not to the dark matter. Even up until $z \sim 100$, a order-unity fraction of the baryons would be coupled to the CMB radiation. In general the gas is significantly hotter than the dark matter and can also have a significant net relative velocity on small scales.

Mass loss is implemented in the toy model via two distinct prescriptions: (1) by dynamically reducing all particle masses according to the PBH evaporation rate ($\dot{M} \sim M^{-2}$) as formulated in Mosbach & Pecker (2022), and (2) a more phenomenological approach where, rather than tracking individual particle masses, we stochastically remove a fixed percentage of particles from the phase-space arrays at each timestep. For simplicity, a spatially flat geometry ($\Omega_k = 0$) was assumed at all times, and simulations ceased at a redshift of $z \approx 1$, the approximate epoch where dark energy begins to significantly influence the cosmic expansion rate and tends to suppress the self-similar growth of structure.

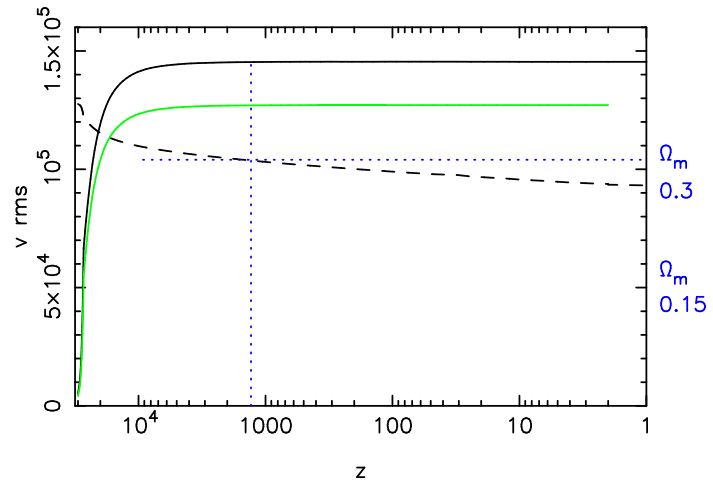


Fig. 2: Evolution of the velocity dispersion of models 102 and 103 (green) with redshift. The dashed line is the fall of density due to dark matter mass loss. If the density is 0.3 at $z = 1300$, at the current epoch it is approximately 0.27, which is within observational uncertainties.

The final large scale structure is illustrated in Figure 3. In spite of the fact that these simulations have orders of magnitude fewer particles, the familiar cosmic web can be traced together with mass concentrations. Note the limitations of the toy model, that there are no baryons, and therefore the stronger mass concentrations, that baryonic collapse and cooling produce, is not seen. The velocity distribution of particles in runs 104–107 is shown in the Appendix. Velocity dispersions are spatially uniform except in the outer parts of the simulations, where particles that have had strong interactions are escaping. These number under 1000 at the final redshift.

3. Normalizing to observations

The simplest bulk flow calculation is to average the velocities of all the particles in the final timestep. This is the PBH bulk velocity, however. A second caveat is that a very few particles have very high velocities due to close encounters and have found their way to very large radii. How small this issue is can be seen by inspection of Figures A1 & A2 in the Appendix. The high velocity tails are scarcely visible. But it is a reason to limit the inclusion radius of the bulk flow calculation.

Figure 2 shows the evolution of that bulk flow velocity field for our fiducial mass-losing run (Run 102) compared to a stan-

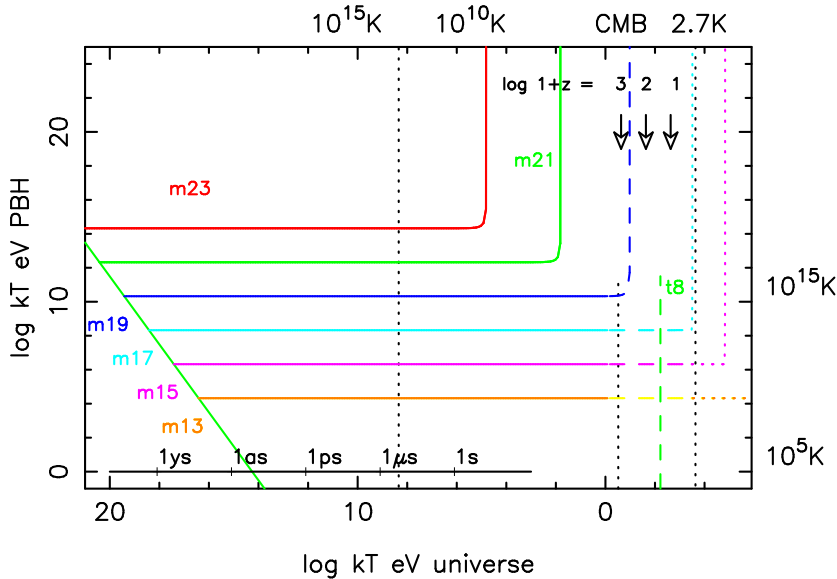


Fig. 1: The temperature evolution of low mass PBHs versus cosmic temperature. In the radiation dominated era PBHs of mass $10^{-23} M_\odot$ (denoted m23) and higher, if they form, do so on the green diagonal line, and evolve with little mass loss until \dot{M} is of the same order as M , at which point they rapidly heat and evaporate. Kelvin units are on the top and right borders. PBHs change their evolutionary rate as $T \sim M^{-1}$, from radiation (solid line), to matter (dashed line), to dark energy dominated (dotted line). The t8 line marks the start of galaxy formation. The three dotted vertical lines are from left to right the QCD transition at 220 MeV, the surface of last scattering of the CMB and the temperature today, 2.7K. The first of these is discussed as a possible PBH trigger by Alonso-Monsalve & Kaiser (2023). As the universe cools, the lowest mass PBHs take a right angle turn to high temperatures, rapidly becoming Planck mass relics. Higher masses are shown by Mould (2025).

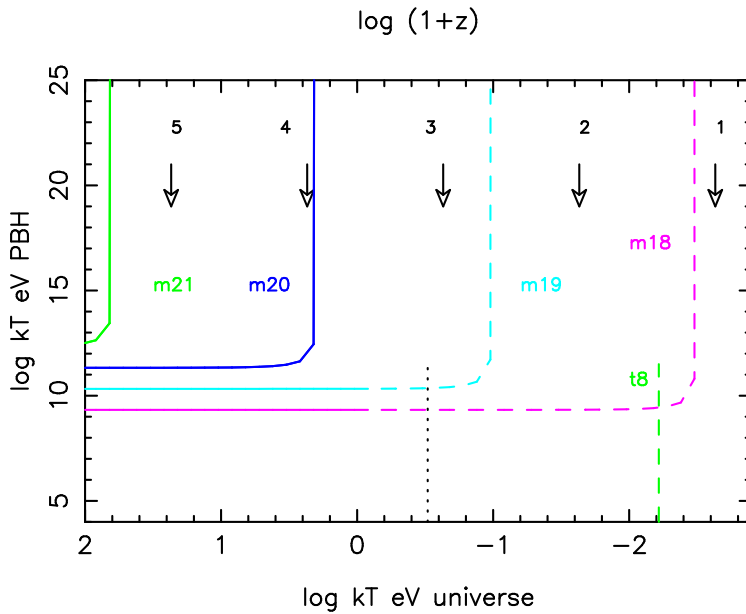


Fig. 1: a. Enlargement of Figure 1 for $z < 10^5$. Redshift $\log(1+z)$ is denoted by the numbers towards the top. The CMB is shown by the vertical dotted line, and 10^8 years by the green vertical dashed line.

110 standard, constant-mass control simulation. The cosmic matter density parameter, Ω_m , is also shown by the dashed curve. In a standard cosmology, Ω_m evolves purely due to cosmic expansion; however, in our model, it also decreases as particles lose mass. The mass loss rate in Run 102 was carefully calibrated so that Ω_m declined by only 10% between the epoch of recombination ($z \sim 1100$) and the present day ($z = 0$). This specific constraint

110 was chosen to ensure our model does not violate late-time cosmological probes, such as the luminosity distances of Type Ia supernovae or the growth of structure inferred from weak lensing, which tightly constrain the recent expansion history (DES 120 collaboration 2024). The quantitative results are summarized in Table 2. The bulk flow, calculated as the median velocity of all

Table 2: Bulk flow of particles

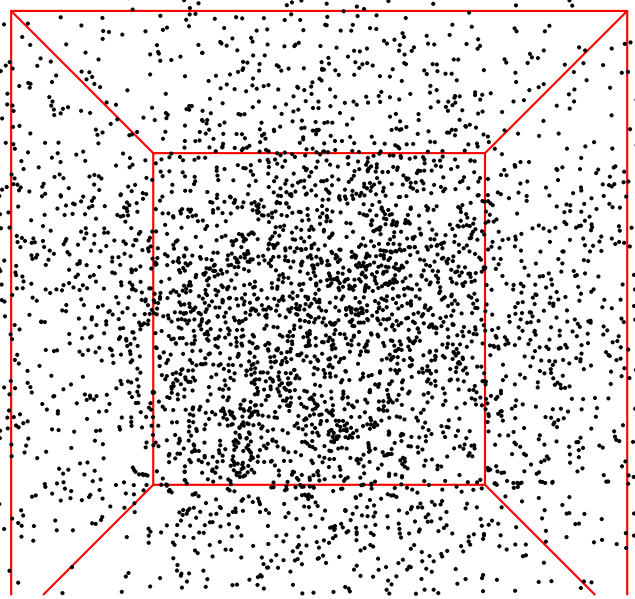


Fig. 3: The central part of run 104, timestep 99 in 3D.

particles within spherical top-hat volumes, is shown for two representative scales.

The first row in Table 2 gives the three components of the bulk flow velocity and the second their uncertainty. The first column in the table gives the number of particles in the calculation. The third row shows the significance 1, 2 or 3σ of the bulk flow measurement. At both large radii (median particle separation) and smaller radii (half that), the mass-losing model generates a bulk flow with an amplitude approximately twice that of the constant-mass model. This statistically significant enhancement arises because the early, higher-density phase allows for greater initial velocity kicks, while the subsequent mass loss reduces the gravitational potential of large-scale structures, preventing these high velocities from being decelerated as strongly as in a standard cosmology. This result is in line with observational tensions, bringing the model's predictions into much closer alignment with the high-amplitude flows of $\sim 400 \text{ km s}^{-1}$ measured on scales $> 100 \text{ h}^{-1} \text{ Mpc}$ (Watkins et al. 2023).

Run 102 included	mass loss total	Vx	Vy	Vz
24720	160577	839	-347	646
	\pm	295	294	287
	σ	2.84	1.18	2.25
109875	160577	625	-666	40
	\pm	177	177	177
	σ	3.52	3.76	0.23
Run 103 included	no mass loss total			
39125	192351	462	-580	-385
	\pm	219	220	216
	σ	2.10	2.64	1.78
178591	192351	341	-345	-145
	\pm	131	131	130
	σ	2.60	2.62	1.11

Velocities are in arbitrary units.
Row σ = ratio of 2 rows above it, indicating the significance.
of particles included within the chosen radius is in column (1).

Table 2 demonstrates that the higher peculiar velocities are indeed attained by the models incorporating mass loss. These and all simulations reported here employed $N=256,000$ particles within a cosmological volume, evolved using the gravitational N-body code of Mould & Hurley (2025). The number of adaptive timesteps required to reach the final state at $z \sim 0$ ranged from 70 to 100.

However, to make a meaningful comparison with observations, one needs to examine the bulk flow velocities of identified dark matter halos, which serve as proxies for galaxies. Two point correlation, followed by 3 point correlation was used, to find (proto)galaxies in the simulations. In practice, this meant finding galaxy pairs separated by the median radius divided by $\sqrt{1000}$, and then forming triangles from these galaxies, whose sides summed to less than the median radius divided by $\sqrt{5000}$. This is a heuristic approach, and it should be compared with the more tested friends-of-friends algorithm.

Although the simulations are inherently scale-free, applying this galaxy finder suggests a physical scale⁴. Setting particle velocities to be in km s^{-1} , with $G = 1$ in the code, then $M = v^2 r$ means that a particle represents $10^8 M_\odot$ and a pixel of distance, r , 0.5 pc. The conclusions below are independent of this normalization. If 100 DM particles are chosen to be the minimum to represent a galaxy, then that galaxy in the toy model is of order $10^{10} M_\odot$. With these considerations in mind, and cognizant of these limitations in the normalization, I present results for the bulk flows of identified halos in Table 3. The row with the run number in Table 3 gives the number of galaxies found (18 in the case of run 111), the bulk flow velocity $\sqrt{(v_x^2 + v_y^2 + v_z^2)}$ (13038 units in the case of run 111) and the starting redshift z_0 . The next row gives the bulk flow velocity components. The third row gives the 1σ uncertainties in the components.

⁴ The most likely mass for PBH DM lies in the asteroid window, which has not been reached by microlensing. Applying a galaxy finder to unite DM particles into halos associates a small number of neighbour particles to represent a galaxy of mass 10^8 to $10^{10} M_\odot$. But they don't become $10^8 M_\odot$ particles. The simulations are scale free in mass, length and time, and the actual particle mass is not specified.

4. Bulk flow of galaxies

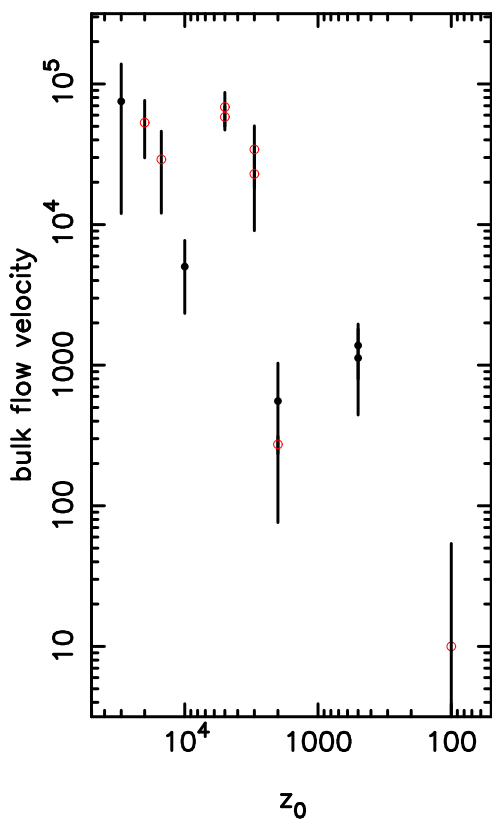


Fig. 4: The resultant bulk flow velocity increased with increasing initial redshift, z_0 . Solid symbols are from Table 3, representing assemblies of dark matter with more than 100 particles. Open symbols are from the Appendix and are unrestricted as to the number of particles. Simulations with mass loss are in red.

It is clear from these results and Figure 4 that starting halo formation from a high-redshift, rather than from linear perturbations at $z \sim 100$ ($t \sim 17$ Myr in a standard cosmology), is the primary driver of the large bulk flows. This presence of collapsed, high-density objects at very early times is a natural property of PBHs. PBHs with masses $M < 10^{-17} M_\odot$ would form from the collapse of large-amplitude primordial density fluctuations at redshifts $z > 10^{10}$, acting as massive seeds for structure formation long before the baryonic Jeans mass would allow for conventional galaxy formation.

PBH formation mechanisms, of which there are many, none of which has the status of a widely agreed model⁵, are not expected to make black holes of a single mass. So it is useful to consider what range of masses lose $\sim 1\%$ per timestep of their mass, typical of the calculations here. This is shown in Figure 5 for the Mosbech & Picker (2022) formula and the redshift range (100, 10000).

⁵ Detection of PBHs is also a matter of debate. In the mass range from stars to asteroids microlensing observers have tended to publish both candidate events and PBH upper limits, e.g. Niikura et al. (2019) and Li et al. (2025).

Table 3: Bulk flow of galaxies with more than 100 particles

run #	galaxies v_x	bulk flow v_y	z_0 v_z	Ω'_m
111	260	7472	33000	98%*
	-1466	6154	-3976	
±	174	543	325	3×10^{-6}
	487	5872	30000	
112	-2707	4137	3168	98%*
	370	300	219	
113	107	1073	10000	98%*
	78	993	400	
±	270	280	256	5×10^{-5}
	404	758	10000	
114	527	-353	-415	98%*
	115	111	65	
115	193	1124	500	0
	443	-620	827	
±	399	300	489	0

* 98% signifies a $< 2\%$ probability that the 3D bulk flow was nonzero by chance.

z_0 is the initial redshift.

† Mass loss method (2)

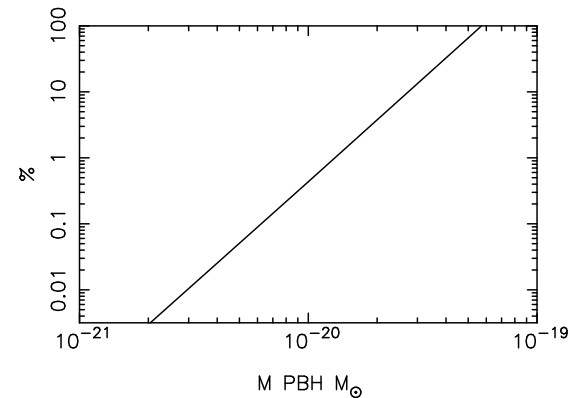


Fig. 5: The percentage of DM required to produce an average 1% mass loss per timestep in one of the runs in Table 1. This takes only a 1% portion of the total DM to have that mass for m20, but 100% for m19.3. The steep slope is because fractional mass loss rates, $1/M dM/dt \propto M^{-3}$.

Various initial mass functions of PBHs are considered in the literature, but that is beyond the scope of the present work.

5. Discussion

Three matters seem well worth further consideration. First, why the bulk flow is affected by PBHs; second, how mass loss is accommodated in the Friedmann equation, and third, how these results should be followed up.

On primordial scales, Silk damping effectively erases baryonic density fluctuations below the photon diffusion scale ($\sim 10^{13} M_\odot$) prior to recombination. Similarly, the free-streaming of certain dark matter candidates like warm dark matter or hot dark

matter smooths the density field on scales up to their respective free-streaming lengths (Sarkar, Sethi & Das 2017). However, there is very little that can retard⁶ the acceleration of PBHs by their mutual gravitational interactions, and the hierarchical clustering and velocity growth of PBHs. As discrete and compact objects, their effective interaction cross-section arises from their small geometric size. Consequently, processes like dynamical friction, which depend on scattering off a sea of lighter background particles, are highly inefficient in an early universe dominated by a population of similarly-massed PBHs.

A very simple physical effect is therefore seen to be at work here. Either because density at redshift of order 10^3 is higher (Figure 2), or because the period for gravitational interaction is longer, or both, the *rms* velocities of the halos that will form galaxies are raised. This combination inevitably raises the velocity dispersion of the PBH population that will later seed galaxy formation. Although we concentrate on PBHs in the present paper, there are other macroscopic DM candidates that precede WIMPs in forming galaxy halos. Axion miniclusters (Kolb & Tsachev 1996, Fairbairn, Marsh & Quevillon 2017) begin their gravitational interactions right at matter/radiation equality, and would share the bulk flow raising properties of PBHs, but not their mass loss.

Allowing Ω_m to vary over some fraction of the lifetime of the Universe is readily accommodated in the Friedmann equation.

$$\left(\frac{H}{H_0}\right)^2 = \Omega_r(1+z)^4 + \Omega_m(1+z)^3 + \Omega_k(1+z)^2 + \Omega_\Lambda, \quad (1)$$

where H_0 is the Hubble constant, and Ω_r , Ω_m , Ω_k , and Ω_Λ are the radiation and matter density, the curvature and cosmological constant relative to the critical density. If we write the changing matter density as $\Omega_m = \Omega_{m0} + \Omega'_m(1+z)$, by analogy with w and w' in time varying⁷ dark energy models, and choose a flat universe, equation (1) becomes

$$\left(\frac{H}{H_0}\right)^2 = (\Omega_r + \Omega'_m)(1+z)^4 + \Omega_{m0}(1+z)^3 + \Omega_\Lambda, \quad (2)$$

That is, Ω'_m is accommodated by increasing the radiation term Ω_r by Ω'_m . This is so, whether or not the evaporating PBH releases 100% radiation, or not. This has the effect of delaying matter radiation equality and requiring a correction to the Planck (2020) value of the Hubble Constant. To preserve the precisely measured angular scale of the sound horizon at last scattering, this change to the pre-recombination expansion history necessitates a compensatory increase in the expansion rate, H_0 , thereby helping to alleviate the Hubble tension. This effect is separate from the impact of the PBH ionization time-bomb (Batten & Mould 2025). For instance, doubling the effective radiation energy density shifts the redshift of last scattering in the Recfast code (Seager, Sasselov & Scott 2000) by $\delta z = 13$, which requires a compensatory H_0 increase of $\sim 1.5\%$.

Although it may appear that this model could be ruled out by next-generation supernova cosmology experiments achieving close to 1% precision in the comparison of Ω_m derived from the

CMB with that from $z = 0 - 2$ probes, it is not so simple. The model possesses sufficient flexibility; for instance, by manipulating the PBH initial mass function to favour higher-mass PBHs (which evaporate more slowly) or by postulating a WIMP half-life that ensures decay is $>99\%$ complete by $z > 1100$, one can engineer a scenario where the mass loss effectively ceases before recombination, leaving the late-time expansion history virtually indistinguishable from Λ CDM.

To robustly verify these early Ω'_m simulations, higher-resolution runs with particle numbers of $N > 10^7$ would be desirable, so that galaxy-mass halos are resolved by thousands of particles rather than hundreds, allowing for a more accurate treatment of halo substructure and merger dynamics. A suite of N-body simulations for the *Euclid* mission (Rácz et al. 2025), extending to wavenumbers of $k \sim 140 \text{ h Mpc}^{-1}$. All of them show the characteristic decline in power on large scales (small k) that is in tension with peculiar velocity surveys (Hoyle, Szapudi & Baugh 2000; Scargle, Way & Gazis 2017). Simulations incorporating the PBH-seeded, mass-losing dark matter mechanism, as outlined here, would be a valuable and timely addition to this effort.

Looking to the future, simulations show that a million redshifts within $z = 0.1$ with *rms* distance uncertainties of 20% will measure a bulk flow to an accuracy of $\pm 11 \text{ km s}^{-1}$. These will be available when DR1 of DESI has been processed for peculiar velocities. These simulations also show that the radius of a bulk flow can be determined with precision⁸. So there is a reasonable expectation that power on large scales can be well measured.

5.1. The Friedmann equation as a fitting function

With the discovery of dark energy the Friedmann equation morphed from an equation relating matter and radiation density to General Relativity's curvature of space to a fitting function. Figure 6 shows the Planck cosmology's fit to the Dark Energy Survey's OzDES supernova distance moduli (Abbott et al. 2024). This can be compared with the distance moduli without dark energy (the red line). The green line is equation (3)

$$\left(\frac{H}{H_0}\right)^2 = \Omega_{m0}(1+z)^3 + \Omega_{ma2}(1+z) + \Omega_\Lambda \quad (3)$$

defining $\Omega_m = \Omega_{m0} + \Omega_{ma2}/(1+z)^2$, which simply uses a different functional form to express mass loss. It is a good fit, but mass loss cannot replace dark energy. What it can do is modify the distance moduli by the 0.075 mag which is the difference been 10% more or less dark energy at $z = 1$. The Planck power spectrum constraint on curvature has been acknowledged by choosing Ω_{ma2} rather than Ω_{ma} . It will be interesting to see if equation (3) can be fitted to DESI's millions of redshifts as well as the dynamic dark energy w_0-w_a cosmology (Roy Choudhury 2025, DESI collaboration 2022). Whether a prescription exists for a PBH IMF that would approximate this fit remains to be seen.

6. Conclusions

To provide more power at large scales we may not need to depart from the Λ CDM paradigm, assuming PBHs can be considered cold dark matter. Just as the DESI collaboration (2025) has

⁶ For a PBH of mass 10^{-10} M_\odot at $z = 10^4$ the stopping distance due to ρv^2 pressure is an extraordinary $10^{50}/\text{m}10 \text{ cm}$. For dynamical friction it is approximately $10^{35} v_{100}^4/\text{m}10 \text{ cm}$, where v_{100} is the velocity in units of 100 km s^{-1} . The radiation pressure exceeds the gas pressure by a factor of 10^9 , but does not change the situation.

⁷ Recent work by the DES and DESI collaborations has favoured w_0 and w_a over w and w' .

⁸ Peculiar velocities must be corrected for Malmquist bias, if the systematic errors are not to exceed the random errors calculated here. This requires attention to the detail of sample selection effects.

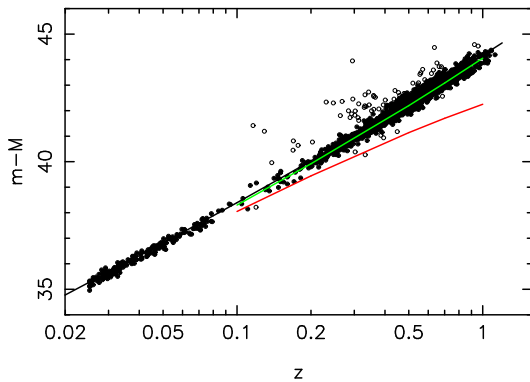


Fig. 6: The currently leading supernova cosmology Hubble diagram of Abbott et al. (2024) (distance modulus versus redshift). Open circles are outliers not used in the fit. The solid line is the Planck cosmology fit; the red curve is the same equation without dark energy, and the green curve is equation (3) with the optimum value of Ω_{m2} .

embraced a time varying w equation of state, parameterized by w_0 and w_a , what is being trialled here with PBHs is a variable Ω_m Λ CDM cosmology. Until we better understand the physics of DM, this may be the closest one can approach to a standard model that can fit bulk flow constraints. These calculations have focussed on PBHs, in part because they involve no new physics, but they apply to decaying DM generally. Cosmological simulations are a mature science, and one should be cautious about results from a toy model, until they have been explored further with dark-matter and gas-plus-dark-matter codes. In the cosmology fitted to the DESI data, the equation of state parameter $w(z) \equiv w_0 + w_a z/(1+z)$. A PBH mass loss parameter should be investigated as a physical alternative to w_a . Finally, simulations starting at or before matter/radiation equality should be explored for axion miniclusters, as these may also produce CMB dipole sized bulk flows.

References

Aaronson, M. et al. 1988, IAUS, 130, 185
 Abbott, T. et al. (DES Collaboration) 2024, ApJ, 973, L14
 Alonso-Monsalve, E. & Kaiser, D. 2023, Phys Rev L, 132, 231402
 Batten, A. & Mould, J. 2025, submitted to MNRAS
 Bertschinger, E. 1998, ARAA, 36, 599
 Böhringer, H. et al. 2025, arxiv 2501.19236
 Bouillot, V., Alimi, J., Rasera, Y. & Füfze, A. 2014, Frontiers of Fundamental Physics & Physics Education Research, Springer Proc. in Physics, 145, Springer Switzerland, p. 89
 Colless, M. 2024, IAUGA, 32, 1950
 Courtois, H. et al. 2025, arxiv 250201308
 Dekel, A. 1993, ASPC, 51, 194
 Di Valentino, E., Perivolaropoulos, L. & Said, J. 2024, Universe, 10, 184
 DES collaboration 2024, ApJ, 975, 86
 DESI collaboration 2025, arxiv 2411.12022
 DESI Collaboration; Abareshi, B. et al. 2022, AJ, 164, 207
 Fairbairn, M., Marsh, D. & Quevillon, J. 1996, PRL, 119,

021101

Hoyle, F., Szapudi, I. & Baugh, C. 2000, ApJ, 317, L51
 Hudson, M. et al. 2004, MNRAS, 352, 61
 Kolb, E. & Tsachev, I. 1996, ApJL, 460, L25
 Li, B. et al. 2025, arxiv 2507.00770
 Lauer, T. & Postman, M. 1994, ApJ, 425, 418
 Mosbech, M. & Picker, G. 2022, SciPost, 13, 100
 Mould, J. 2025, ApJ, 984, 59
 Mould, J. & Hurley, J. 2025, arxiv 2509.02165
 Niikura, H. et al. 2019, Nature Astronomy, 3, 524
 Pérez de los Heros, C. 2020, Symm, 12, 1648
 Planck collaboration 2020, A&A, 641, A6
 Poulin, V., Desgourges, J. & Serpico, P. 2017, JCAP, 3, 43
 Rácz, G. et al. 2025, A&A, 695, 232
 Roy Choudhury, S. 2025, ApJ, 986, L31
 Sarkar, A., Sethi, K. & Das, S. 2017, JCAP, 7, 12
 Scargle, J., Way, M. & Gazis, P. 2017, ApJ, 839, 40
 Scrimgeour, M. et al. 2016, MNRAS, 455, 386
 Seager, S., Sasselov, D. & Scott, D. 2000, ApJS, 128, 407
 Secrest, N. et al. 2025, arxiv 2505.23526
 Taylor, E.N. et al. 2023, ESO Messenger, 190, 46
 Tsagas, C., Perivolaropoulos, L. & Asvesta, K. 2025, arXiv:2510.05340
 Tully, R.B. 1989, ASSL, 151, 41
 Watkins, R. et al. 2023, MNRAS, 524, 1885
 Whitford, A. et al. 2023, MNRAS, 526, 3051

330

340

350

Acknowledgements

The ARC Centre of Excellence for Dark Matter Particle Physics is funded by the Australian Research Council through grant CE200100008. Simulations were carried out on Swinburne University's Ozstar & Ngarrgu Tindebeek supercomputers, the latter named by Wurundjeri elders and translating as "Knowledge of the Void" in the local Woiwurrung language. I would like to thank the organizers of *Cosmic Flows 2025* for a conference that informed and inspired this paper. I am grateful to Darren Croton for helpful advice and also to the journal editor and referee. Google Gemini Pro 2.5.0 helped to render this paper more readable. Thanks to Tamara Davis for supplying the OzDES supernova data.

360

Code availability

Suitable n-body codes are reviewed by Bertschinger (1998), and thanks to Michael Blanton for the visualization code P3D.

Appendix

Boundary conditions

370 The n-body code used here was written to investigate the formation of dark clusters from PBH. The particles expanded into a vacuum. The same code (Mould & Hurley 2025) is used here. Normally, cosmological simulations have periodic boundary conditions to preserve homogeneity and isotropy, in contrast to the present simulations which deviate from homogeneity at the distances of the furthest particles. This was investigated by re-running simulation 103 with reflective boundary conditions, in which the simulation is contained in a box which expands with the scale factor. Particles penetrating the box have their velocities reflected. The modified run 103 differed from the original rms velocity by 5%.

380

Additional simulations

Simulations in which less than 100 particles per galaxy were available are summarized here. The final velocity distribution

Table A1: Bulk flow of galaxies (< 100 particles)

run# z ₀	v _x σ _x	v _y σ _y	v _z σ _z	bulk flow velocity	# of galaxies
106	-18059	1338	29063	34243	36
3000*	± 9848	11892	12324	98%	
107	10891	19740	-3998	22897	50
3000	± 7648	10496	6646	96%	
109	106	379	68	399	90
10000*	± 109	84	66	98%	
110	-155	38	-91	184	59
10000	± 250	87	54	87%	
118	-384	168	365	556	21
2000	± 353	284	228	96%	
119	-933	-908	-457	1380	53
500	± 291	374	421	98%	

* Mass loss method (1)

functions of runs 104-107 are shown in Figures A1 and A2.

Dynamic dark energy

The current DESI cosmology is compared with mass losing DM in Figure A3.

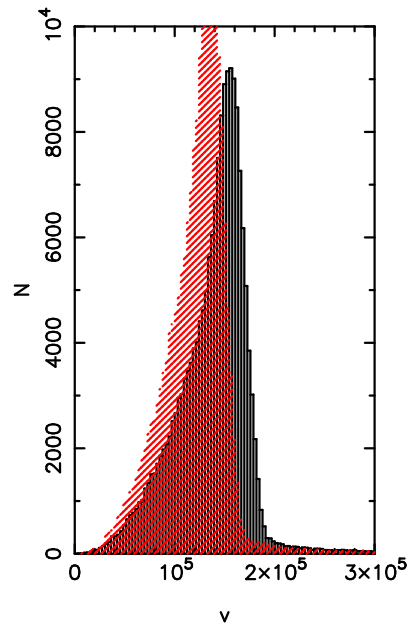


Fig. A1: Velocity distribution functions for run 104 and run 105 (red).

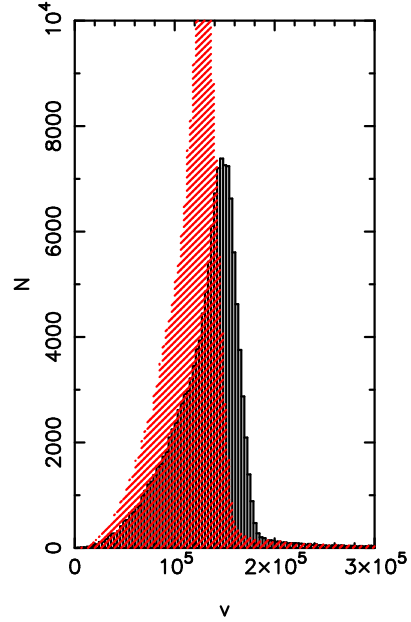


Fig. A2: Velocity distribution functions for run 106 and run 107 (red).

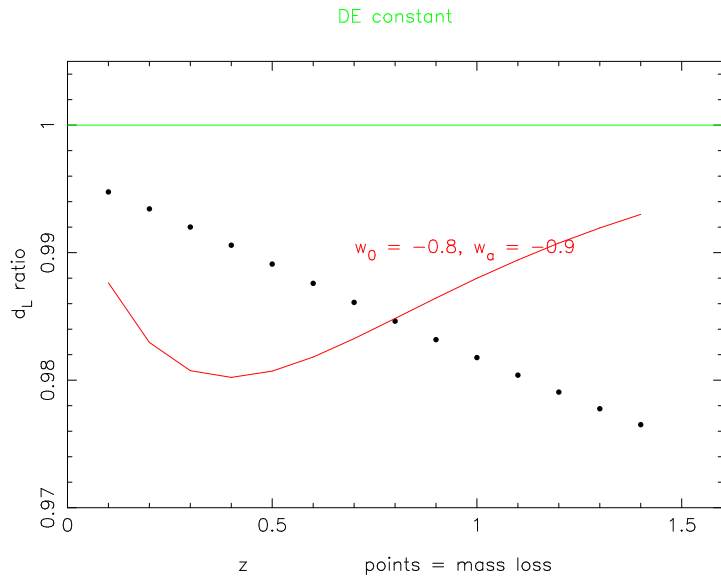


Fig. A3: The remarkable small difference between galaxy luminosity distances due to dynamic dark energy. Distances are ratioed to static dark energy (the green line). The red curve is the cosmology of Abdul Karim et al. (2025). Its turnaround is due to matter domination for $z > 1$. The points are for DM mass loss with $\Omega'_m = 0.015$. They do not turn around because Ω'_m is still effective at $z > 1$. That could be remedied by suitable choice of a PBH IMF.